# Accepted Manuscript

The versatile electron microscope: An ultrastructural overview of autophagy

Joanna Biazik, Helena Vihinen, Tahira Anwar, Eija Jokitalo, Eeva-Liisa Eskelinen

Please cite this article as: J. Biazik, H. Vihinen, T. Anwar, E. Jokitalo, E-L. Eskelinen, The versatile electron microscope: An ultrastructural overview of autophagy, *Methods* (2014), doi: http://dx.doi.org/10.1016/j.ymeth.2014.11.013

**The versatile electron microscope: an ultrastructural overview of autophagy**

Joanna Biazik[1], Helena Vihinen[2], Tahira Anwar[1], Eija Jokitalo[2] and Eeva-Liisa Eskelinen[1]

[1]University of Helsinki, Finland; Department of Biosciences; Division of Biochemistry and Biotechnology, [2]University of Helsinki, Finland; Institute of Biotechnology; Electron Microscopy Unit.

*Corresponding author: eeva-liisa.eskelinen@helsinki.fi

Department of Biosciences, Division of Biochemistry and Biotechnology

PO Box 56, 00014 Helsinki, Finland

Delivery/courier service address:

Viikinkaari 5D,Bio2, Room 4022, 00790 Helsinki, Finland

Tel. +358 2941 59566, Fax +358 2941 59068

joanna.biazik@helsinki.fi; helena.vihinen@helsinki.fi; tahira.anwar@helsinki.fi;

eija.jokitalo@helsinki.fi

**Abstract**

Both light microscopy (LM) and electron microscopy (EM) are able to reveal important information about the formation and function of various autophagic compartments. In this article we will outline the various techniques that are emerging in EM, focusing on analyzing three-dimensional morphology, collectively known as volume electron microscopy (volume EM), as well as on methods that can be used to localize proteins and antigenic epitopes. Large cell volumes can now be visualized at

the EM level by using one of the two complementary imaging techniques, namely Serial Block-face Scanning Electron Microscopy (SB-SEM) or Focused Ion Beam Scanning Electron Microscopy (FIB-SEM). These two block-face imaging methods reveal ultrastructural information from all membrane-bound organelles such as autophagic compartments to be visualized in a three-dimensional space, in association with their surrounding organelles. Another method which falls into the volume EM category is dual-axis electron tomography (ET). This method is more suited to reconstructing smaller volumes from areas of interest that require nano-structural detail to be confirmed such as membrane contact sites (MCSs) between autophagic compartments and various organelles. Further to this, to complement the morphological identification of autophagic compartments, immunolabeling can be carried out at the EM level to confirm the nature of various autophagic compartments depending on the localization of various antigens at a sub-cellular level. To determine this, various immunolabeling techniques can be carried out, namely the pre-embedding or the post-embedding immunolabeling methods. Examples of both of these methods will be described in this chapter. Correlative light-electron microscopy (CLEM) can be used to visualize the same autophagic organelles under the LM, followed by high-resolution imaging under the EM. Finally, cryofixation has revolutionized the EM field by allowing rapid immobilization of cells and tissue in the near native state, so samples are no longer prone to artefacts induced by chemical fixation. Collectively, this chapter will discuss the aforementioned capabilities of the EM in more detail, with a particular focus on autophagy, namely the impact of EM in the study of the morphology and biogenesis of the phagophore/isolation membrane (referred to as the phagophore hereafter).

**Highlights:**

- block-face imaging techniques yield three-dimensional data of relatively large volumes with ultrastructural resolution

- dual-axis electron tomography resolves nano-structural detail of smaller volumes

- CLEM and immunoEM assist in ultrastructural localization of proteins

- high-pressure freezing followed by freeze substitution yields excellent ultrastructural preservation

## 1.1 Imaging volume with ultrastructural resolution

Until recently it has been difficult to get three-dimensional information on cell and tissue structure over tens of micrometers with a resolution sufficient enough to identify membrane-bound organelles such as autophagic compartments and their surrounding structures such as mitochondria, endoplasmic reticulum (ER), endosomes, lysosomes and the Golgi complex. To overcome this issue volume electron microscopy (volume EM) [1] offers various novel techniques which allow for large cell volumes to be sampled. Two of these techniques utilize the low accelerating voltages of the scanning electron microscope (SEM). Commonly, SEM has been used to scan the surface of samples with a secondary electron detector to reveal topographical information about the specimen such as microvilli or ciliated protrusions [2], thus it has not been very useful for scanning the featureless flat

surface of resin-embedded blocks. The SEM has since evolved to produce two systems that use backscattered electron detectors to image the surface of resin-embedded sample blocks that have been heavily contrasted with osmium. The sample block is mounted onto a platform in the chamber of a scanning electron microscope. Both techniques work on a similar principle whereby the block face of a plastic-embedded sample is repeatedly removed and discarded from the block, either by a diamond knife (SB-SEM) or by a focused ion beam (FIB-SEM). The exposed block face is sequentially scanned using an electron beam operating at a low voltage, i.e., 1-3 kV, and a backscatter electron detector is used to visualize the heavy-stained block face. In the case of SB-SEM the microscope chamber is equipped with a built-in ultramicrotome which sequentially cuts 40-nm thick sections of the block (Fig. 1A-C). The hardness of the resin is critical as harder resins take up more stain and can withstand a higher dose of electrons, therefore improving sectioning and scanning capabilities [3], with some reports claiming that extremely thin (5 nm) sections can be achieved [4]. The first such application of a built-in microtome was seen as early as 1981 [5], however each time the microtome sectioned the block face, the chamber had to be re-opened and the sample had to be re-coated with a conductive layer. Furthermore storage space for such large data sets was also limited during the advent of these machines [5], hence no volumetric data eventuated from these earlier studies. Technology has since made the modern machines more automated and currently the main physical constraint of SB-SEM is the limitation imposed by the cutting surface of the diamond knife, which is 800 $\mu m^2$, however the total volume that can be achieved is very large ranging from 1000 $\mu m^3$ to 1,000,000 $\mu m^3$ with a lateral resolution of ~5 $nm^2$ [1]. This results in the automated acquisition of a stack of hundreds of perfectly aligned images which can be

4

generated for the whole cell volume [6], exceeding thicknesses greater than 20 μm (Fig. 1D) . The slices can be assembled into volume files using various available software, in our case IMOD [7] (Figs. 1D, 2). In our case, segmentation of structures to reconstruct three-dimensional models is done manually by tracing the organelles or regions of interest in all the consecutive slices by hand. Automated segmentation methods are currently under development.

The other method which generates volumetric data using a block-face imaging technique is FIB-SEM. This method is very similar to the aforementioned SB-SEM, however, it relies on precise ablation of material from the specimen surface using a focused ion beam [8] instead of sectioning using a diamond knife as is the case in SB-SEM. Therefore, FIB-SEM can generate a milling thickness of approximately 18.9 nm [9, 10]. FIB-SEM can also accept higher electron doses thus improving the axial resolution to ~ 3nm [1]. The volumes that can be imaged with FIB-SEM are typically smaller than those imaged by SB-SEM and range from <10 $\mu m^3$ to 10,000 $\mu m^3$. Ion beam milling is also much slower than SB-SEM sectioning, hence the high resolution of FIB-SEM comes at the expense of speed [1]. Nonetheless, as is the case with SB-SEM the whole scan is automated and it does not require any alignments of serial sections or serial images as drift between successive sections is minimal [9]. Autophagy-related vacuoles have been identified using this method in the brain of *Drosophila* Alzheimer´s disease model [10]. That same study also claims that the double membrane of the autophagosome can be resolved using the FIB-SEM method [10], however in the case of SB-SEM, we have been unable to make a distinction between the two membranes of the phagophore or autophagosome [11]. Despite this limitation, phagophores and autophagosomes can

be identified in SB-SEM based on their morphology and selective contrasting with reduced osmium tetroxide.

Collectively, these two block-face imaging methods allow for a reconstruction of volumetric data at the resolving power of an electron microscope and have proven to be very effective in the field of autophagy, particularly in the area of phagophore biogenesis. SB-SEM and FIB-SEM allow for the identification of the heavily osmium-stained c-shaped phagophore and more importantly its close relationship with other organelles, to help determine which organelles are potentially supplying membranes to the phagophores during their biogenesis and growth [11]. Even though this method allows you to clearly distinguish a phagophore from an autophagosome or an endosome by morphology, the resolving power of SB-SEM and FIB-SEM is not adequate enough to help resolve smaller nano-structural detail like membrane connections [12] between phagophores and other organelles. Such membrane connections have been previously reported between the phagophore membrane and the membrane of the ER with dual-axis ET [13, 14] or between the phagophore and an ER-mitochondria contact sites with conventional transmission EM [15]. Furthermore, as growing molecular studies are revealing that other organelles could also be making contacts with the phagophore, and more importantly, that lipid transfer is indeed active at MCSs [16], it is important to investigate these organelles in further detail. So to verify whether MCSs are present between the phagophore membrane and organelles that have been previously identified by SB-SEM or FIB-SEM to be in close communication with the phagophore, then electron microscopy offers another technique, namely dual-axis electron tomography (ET).

### 1.2 Nano-structural detail and membrane connections

Tomography is another volume EM method which is used for reconstructing the interior of an object from its projections [17]. In dual-axis ET [18] a 250-nm thick resin section is tilted for example over ± 62$^o$ in an electron tomography holder around two orthogonal axis. As the holder is tilted one degree at a time an image is taken and when the whole tilting sequence (over 125 images) is complete the back projection of the acquired images allows for segmentation of the volumetric data and three-dimensional modelling to be carried out (Fig. 3). At nominal magnifications of 10,000x each slice of the tomographic sequence is 1.6 nm thick and reveals intricate ultrastructural detail of organellar structures, such as MCSs, which would be overlooked with routine EM (Fig. 3B-C, E-G). It is obvious that the volume obtained with dual-axis ET is limited compared to SB-SEM and FIB-SEM. However, dual-axis ET can be used to reconstruct larger volumes by acquired tilt series from consecutive 250-nm sections, and then joining the tomograms together. The corresponding region has to be found in each of the 250-nm sections when viewed with the electron microscope and then, after the tilt series have been performed for each of the sections, the alignments and reconstructions of the tomograms is carried out using computer software. Serial-section dual-axis ET has been readily implemented in our laboratory to generate final volumes of 12 $\mu$m$^3$ of cytoplasm [14], and more importantly volumes that are thick enough to contain a whole autophagic compartment such as the phagophore. This technique has already shown that the regions of the ER cisternae found next to the forming phagophores, makes one [13] or several connections [14] with the phagophore membrane, thus implicating the ER in initial phagophore biogenesis.

To summarize the volume EM methods described above, dual-axis ET achieves high z-axis resolution but the volumes that can be imaged are relatively small. On the other hand, FIB-SEM and SB-SEM have limited z-axis resolution but larger volumes can be visualized, especially when using SB-SEM.

### 1.3 Immunolabeling at EM level

Identifying the subcellular location of antigens has been very important for functional cell biology studies. All membrane-bound autophagic compartments are visible when viewed with the electron microscope, and more importantly the autophagic compartments can be morphologically identified to determine whether they are phagophores, autophagosomes, or degradative autophagic vacuoles/autolysosomes [19, 20]. To complement and extend the morphological data, immunolabeling can also be carried out at the EM level. Many different protocols have been developed for immunolabeling, including pre-embedding and post-embedding immuno electron microscopy (immunoEM). In pre-embedding immunoEM, the antibody incubations are carried out with whole cells or tissue slices, while in post-embedding immunoEM, antibodies are applied to thin sections picked up on EM grids. In this review, we will describe one pre-embedding method that has been applied in several recent autophagy studies, namely pre-embedding immunoEM with nanogold-conjugated secondary antibodies. In addition, we will shortly describe a widely used post-embedding technique, the Tokuyasu cryosection method. We will also discuss the advantages and disadvantages of these two approaches.

Horseradish peroxidase (HRP) conjugated secondary antibodies have been used in pre-embedding immunoEM, and their advantage is sensitivity due to

amplification of the label by the enzyme activity. HRP activity is visualized with diaminobenzidine (DAB) that in the presence of $H_2O_2$ forms an insoluble osmiophilic precipitate. The drawback of the HRP-DAB method is poor resolution of the label, which in addition has the tendency of masking delicate ultrastructural details. However, since the introduction of secondary antibodies conjugated to 1.4 nm nanogold particles and silver enhancement protocols, pre-embedding immunogold labeling [21] has proven to be a favorable method resulting in good preservation of ultrastructure and excellent labeling intensity (Fig. 4). It has been shown that the size of the conjugated gold particles is inversely proportional to the labeling efficiency, hence the best efficiency is achieved with smallest possible gold particle size [22]. In the nanogold pre-embedding method we have found that antibodies that yield good fluorescent labeling at the LM level using 4% paraformaldehyde as a fixative will most likely yield good labeling at the EM level. The protocol requires an initial fixation in 4% paraformaldehyde, followed by quenching of aldehyde groups with glycine and permeabilization of the cell membranes using a mild saponin buffer. LC3 labeling can be used to identify phagophores and autophagosomes. Good antibodies to LC3 are available commercially, and manufacturer's instructions (Anti LC3, Clone LC3.1703 Cosmo Bio) suggest an additional permeabilization step, carried out by immersing the cover slips with cells into liquid nitrogen after fixation (Fig. 4A-C). The cells are then immunolabeled with primary antibody, followed by a secondary antibody that is conjugated to 1.4 nm nanogold particles. Since these particles are very small and not readily visible when viewed with the EM, a silver enhancement protocol is required to amplify the small 1.4 nm gold signal. The silver enhancement should be performed in a darkroom under red light. This is followed by a gold toning step, also performed in the dark room, which is necessary to stabilize the silver

9

particles when viewed with the electron beam. Gold enhancement, rather than silver enhancement can also be used to bypass the final toning step. Signal enhancement is followed by routine osmication, or reduced osmium staining, dehydration, infiltration with resin and polymerization. Although this pre-embedding immunolabeling method requires the purchase of various enhancement kits, chemicals for gold toning and access to a dark room, nonetheless, this technique is quite effective. The mild permeabilization minimally affects membrane ultrastructure and is effective enough to permit penetration of the small 1.4 nm nanogold particles, even across the double membrane of autophagic compartments. Furthermore, with this method you can generate good contrast and most importantly very good labeling efficiency, particularly when longer silver enhancement times are applied (~5 minutes) (Fig. 4).

The pre-embedding method has several advantages. It resembles immunofluorescence labeling of cell monolayers or tissue slices and thus these LM methods can be used to test the suitability of different fixation and permeabilization methods for labeling. Pre-embedding methods do not require any special equipment apart from a routine ultramicrotome, and sectioning of the plastic-embedded samples does not require specific skills on top of routine ultramicrotomy. As described above, labeling efficiency with nanogold conjugates is generally very good. The thin sections and sample blocks can be stored at room temperature for decades, and additional sections can be prepared if needed. However, pre-embedding immunoEM is not well applicable for double-labeling immunoEM. Another drawback can be that the necessary permeabilization step causes damage to some delicate ultrastructural details.

In Tokuyasu cryosectioning [23], the cells or tissue blocks are first fixed in a mild fixative, usually 2-4% paraformaldehyde with or without a low percentage of glutaraldehyde, depending on the epitopes and antibodies to be used. The samples are then embedded in 10-12% gelatin that gives support during the mounding and cryosectioning steps. The samples are next infiltrated in a cryoprotectant such as 2.1-2.3 M sucrose, cut into small blocks, mounted on cryoultramicrotome sample holders, and plunge frozen in liquid nitrogen. Sections are cut in a cryoultramicrotome at -100-120 °C and picked up using a loop with a mixture of sucrose and methyl cellulose. The sections melt on the surface of the pickup solution and are then mounted on EM grids for immunolabeling. Grids with sections covered by the pickup solution can be stored at +4 °C for several months, or even years, before immunolabeling. The sample blocks can be stored under liquid nitrogen for several years. Several excellent papers have been published that describe this method and the improvements that have been developed to enhance the preservation of ultrastructural details of autophagosomes [24-28] and other organelles.

Tokuyasu cryosectioning is fast compared to pre-embedding immunoEM and the labeled sections are ready for inspection one or two days after fixation of the cells, while the pre-embedding methods take 2-4 days to reach the same stage. Since in Tokuyasu method the samples are not embedded in plastic, the epitopes are not masked by the embedding medium. Thus, compared to other post-embedding immunoEM methods such as Lowicryl-embedded sections, Tokuyasu cryosections are more sensitive. Depending on the size of the gold conjugates used, the conjugates can either label the epitopes on surface of the cryosections or penetrate the sections to some degree. Robinson et al. showed that while 1.4-nm

gold conjugated antibodies are able to penetrate 1-2 µm slices of cells, 5-nm gold

conjugates did not penetrate at all and only reached the epitopes on the surface of

the slices [29]. Thus, when using nanogold conjugates, it can be assumed that the

sensitivity of Tokuyasu cryosections is similar or better than in the pre-embedding

method. All post-embedding methods have one prominent advantage over pre-

embedding methods: they allow double and even triple labeling. The most widely

used approach is to use different sizes of gold particles (e.g., 5-nm, 10-nm, and 15-

nm gold). Of note, Tokuyasu cryosectioning has been used in combination with dual-

axis ET [30] and CLEM [31].  A protocol has also been developed where high-

pressure freezing and freeze-substitution can be combined with rehydration,

Tokuyasu cryosectioning and immunogold labeling [32]. This protocol thus combines

the advantages of cryofixation with high-resolution immunoEM.

Tokuyasu cryosectioning, however, needs special equipment, namely a

cryoultramicrotome and a special cryo diamond knife. Further, the ultrastructural

preservation in Tokuyasu cryosections is heavily dependent on the quality of the

sections. Since the samples are not embedded in plastic, and the sectioning is

carried out dry at low temperatures, the sections are very fragile and sensitive to

mechanical damage during sectioning, section manipulation on the knife, and section

pickup and melting. Some laboratories are able to produce excellent ultrastructural

preservation and labeling efficiency using Tokuyasu method [24, 26, 27, 33].

However, it may be that to achieve such excellent section quality, you need to have

this technique in routine use to keep up the sectioning skills. Another disadvantage

of Tokuyasu method is that the contrast of the samples tends to be low, especially if

the post-sectioning osmication is not applied [27]. Thus, membranes will appear

white instead of black, and ribosomes are not visible at all. This makes identification

of autophagic structures difficult; however, this can be circumvented by immunolabeling of autophagic marker proteins such as LC3.

### Correlative light-electron microscopy: different approaches

Although cell dynamics will probably never be captured with the EM, there is one method that combines the ability of light microscopes to visualize fluorescent proteins in living cells and the ability of electron microscopes to resolve ultrastructural detail. That method is called correlative light-electron microscopy (CLEM). As the name suggests, this method is essentially a union of the two imaging platforms. This approach has been successfully used for decades, however, it has gained more popularity in the last 15 years with the application of green fluorescent protein (GFP) -based video microscopy [34]. In many cases, a few seconds of time-lapse video using a GFP-labeled protein had the ability to answer more questions than several years of static microscopy imaging of fixed cells [34, 35]. This clearly demonstrates the importance of LM and more importantly, of live-cell imaging. However, the one main drawback of live-cell imaging is that one fluorescent spot can represent one organelle, an organelle subdomain or aggregates of proteins or membranes [36]. Hence the need still remains for ultrastructural resolution using the EM. CLEM can also be done using fixed cells for both LM and EM. Fix-cell CLEM has been readily employed in the field of autophagy [37, 38]. Of note, another limitation of the CLEM technique which utilizes fluorescently tagged proteins is that in most cases you are visualizing the subcellular domains using proteins that are over expressed, which may cause artefacts.

As stated above, CLEM can also be performed without live-cell imaging, using fixed cells for both LM and EM. There are various commercially available

immunoprobes for CLEM; one such probe is fluoronanogold whereby both a fluorescent dye and 1.4-nm gold particles are conjugated to the secondary antibody. In this method the fluorescent dye is readily visible with the fluorescence microscope and after LM visualization, the 1.4-nm gold particles have to be silver enhanced to improve the signal when visualized with the EM [39]. Another probe which produces fluorescence and EM contrast is a genetically encoded tag called miniSOG (for mini Singlet Oxygen Generator) [40]. MiniSOG is fluorescent, and its fluorescence can be used to generate oxygen radicals that react with DAB, which is then visible in the EM as an osmiophilic precipitate. The fluorescence of MiniSOG fades relatively quickly, making it less ideal for live-cell imaging. However, MiniSOG is effective at preserving high quality ultrastructural information making this CLEM probe compatible with advanced EM techniques including dual-axis ET and SB-SEM, as genetic labeling methods overcome many issues that are associated with permeabilization and penetration of probes into the cells [40, 41]. As already mentioned above, acquisition of tomographic data has also been successful using immunogold-labeled 250-nm thick Tokuyasu cryosections [31]. Furthermore, this same study also generated dual-axis ET data in association with CLEM. This was achieved by tracing the fluorescent signal into the EM by staining nuclear and mitochondrial DNA with a Hoechst stain and using prominent morphological landmarks within the cell to assist in the correlation [31].

### 1.4 Fixation in the near-native state

The main objective of sample preparation for EM has been to dehydrate the sample to remove all the water. Since the discovery that vitreous ice can be sectioned into thin slices which can then be viewed with the EM, it became possible

14

to investigate the potential artefacts caused by chemical fixation [42]. The introduction of cryofixation methods has produced ultrastructural preservation of a superior quality with the added advantage of being able to capture short-lived cellular processes such as vesicle budding and membrane fusion intermediates that cannot be immobilized by the chemical fixatives. Capturing dynamic events is of great importance to cellular biology; hence cryofixation surpasses the immobilization properties of chemical fixation that in addition to being slow, can also introduce structural artefacts.

There are many commercially available units that carry out cryofixation of EM samples including high-pressure freezers, plunge-freezers and vitrobots with a similar range of TEMs equipped with cryo-sample holders as well as cryoET, all of which have capabilities to minimize artefacts associated with chemical fixation. Cryofixation using high-pressure freezing (HPF) followed by automated freeze substitution (AFS) is becoming the fixation of choice for many morphologists. Cell monolayers growing on sapphire discs (Fig. 5A) can be frozen into vitreous ice [42] within seconds of leaving the cell culture incubator (Fig. 5B), maintaining the overall physiological properties, short-lived structures and true shape of cellular organelles (Fig. 5D). Following HPF, the samples then undergo an overnight AFS cycle whereby vitrified water is replaced by organic solvent at very low temperatures (-95$^{\circ}$C). The organic solvent is often supplemented with chemical fixatives or heavy metal salts such as uranyl acetate or osmium tetroxide (Fig. 5C). Taken together, this form of cryofixation  is regarded as being practically free of artefact formation [43]. Cryofixation is also less likely to affect antigenicity of immunoEM samples. However, it should be kept in mind that the embedding medium, such as Lowicryl, needed for thin sectioning of the cryofixed immunoEM samples, is likely to cover at

least part of the antigenic sites. For morphological observations, the cryofixed and freeze-substitute samples can be embedded in normal epoxy resin. The ultrastructural preservation achieved with this method gives improved resolution at a nano-level, which is essential when identifying membrane connections between the phagophore and other organelles.

**Materials and Methods**

In this chapter, we give detailed protocols for those methods that we currently use in our laboratory, namely SB-SEM, dual-axis ET, pre-embedding immunoEM and CLEM. For protocols of Tokuyasu cryosectioning, we recommend the references from those laboratories that have been able to produce excellent ultrastructural preservation with this method [24, 26] .

**2.1 SB-SEM**

Cells were grown on Thermanox cover slips or sapphire discs in 3-cm dishes to subconfluency. The cells were fixed in 2% glutaraldehyde in 0.1 M sodium cacodylate buffer, pH 7.4, postfixed using a reduced osmication method [44], and embedded in resin (Durcupan ACM, Fluka) between two cover slips [45]. The block was trimmed and glued on the microtome sample holder, and imaged with a 2.5 kV beam voltage using a backscattered electron detector (Gatan) in a FEG-SEM Quanta 250 microscope (FEI Company). The microscope chamber was equipped with an ultramicrotome (3View, Gatan Inc.) which allowed for serial sectioning (40 nm sections) of the block face. Images of the block face were captured using Gatan Digital Micrograph software and IMOD software was used to segment each slice by hand to generate a three-dimensional models of the organelles in the image stack.

For FIB-SEM sample preparation and data acquisition please refer to
the materials and methods section in [10].

### 2.2 Dual-axis ET

Cells were grown on 3-cm dishes containing glass cover slips to
subconfluency. The cells were fixed in 2% glutaraldehyde in 0.1 M sodium
cacodylate buffer, pH 7.4, postfixed in reduced osmium tetroxide, and flat embedded
in epon [20]. Semithick 250-nm sections were prepared and picked up on single slot
grids. Colloidal gold particles, 10 nm in diameter, were placed on the top and bottom
of the sections to serve as fiducial markers for alignment of the tomograms. Dual-
axis tilt series were acquired using SerialEM software [7] running on a Tecnai FEG
20 microscope (FEI, Comp) operating at 200 kV with a nominal magnification of
19,000x giving a final pixel size of 0.56 nm. Images were recorded at 1 degree
intervals for the a-axis and 1.5 degree intervals for the b-axis with a 4 k x 4 k CCD
camera (Gatan Inc., USA) over a tilt range of ±62 degrees. IMOD software was used
to create three-dimensional reconstructions (Fig. 3) from the tilt series and to create
models of the membranes [46].

### 2.3 Pre-embedding immunoEM

Immunolabeling was carried out in accordance with two modified pre-
embedding methods [47, 48]. Cells were grown on glass coverslips to subconfluency
and fixed in 4% paraformaldehyde in 0.1 M phosphate buffer (PB, pH 7.4) for 1 h at
room temperature. After washing with PB, free aldehyde groups were quenched with
4% glycine in PB for 10 minutes. The cells were then dipped in liquid nitrogen (in
accordance with manufacturer's instructions, Cosmo Bio, CTB-LC3-2-IC) and

blocked with 5% bovine serum albumin (BSA), 5% normal goat serum, 0.1% cold

water fish skin gelatin and 0.005% saponin in PB. The cells were labeled with mouse

monoclonal anti-LC3 (Cosmo Bio, CTB-LC3-2-IC) or rabbit polyclonal anti-rat LAMP-

1 (gift from Yoshitaka Tanaka, Kyushu University, Japan) at room temperature for 1

h. Cells were washed in PB containing 0.01% saponin and 0.1% BSA and incubated

in goat anti-mouse or anti-rabbit IgG conjugated to 1.4-nm gold particles

(Nanoprobes, 142002, 142004). Cells were washed with PB and fixed with 1.5%

glutaraldehyde in PB for 10 min. After washing, the gold labeling was intensified by

using a HQ silver enhancement kit (Nanoprobes, 2012) and gold toning was

performed to stabilize the silver enhancement by subsequent washes in 2% sodium

acetate, 0.05% gold (III) chloride trihydrate  and 0.3%  sodium thiosulphate

pentahydrate (Sigma, S2889; G4022 and S292 respectively). After washing in

distilled water, cells were postfixed in 1% $OsO_4$ containing $K_4[Fe(CN)_6]$ (15mg/ml) in

0.1M sodium cacodylate buffer at room temperature for 1 h, washed in distilled

water, dehydrated with a graded series of ethanol, infiltrated with resin (Epon, TAAB)

for 1 h and polymerized at +60$^{\circ}$C overnight. Ultrathin sections were collected onto

pioloform coated grids, post stained with uranyl acetate and lead citrate and viewed

using Tecnai 12 (FEI Company) electron microscope.

### 2.4 CLEM with fixed cells expressing a GFP-tagged protein

Cells expressing a GFP-tagged protein were grown on gridded glass-

bottom culture dishes (MatTek Co., MA, USA) and fixed in Karnovsky fixative (2%

paraformaldehyde, 1.5 % glutaraldehyde in 0.1 M sodium cacodylate buffer, pH 7.4)

for 20 minutes. After washing with 0.1 M sodium cacodylate buffer, the culture dishes

were imaged using phase contrast optics to visualize the grid on the dish, and

18

fluorescence microscopy to visualize the GFP signals. These photos were later used to locate the cells of interest in the EM block. Cells were postfixed in 1% $OsO_4$ containing $K_4[Fe(CN)_6]$ (15mg/ml) in 0.1M sodium cacodylate buffer at room temperature for 1 h, washed in distilled water, and dehydrated with a graded series of ethanol and finally with acetone. Then a BEEM capsule filled with resin (Epon, TAAB) was placed upside down onto the area of interest on the culture dish, using the phase contrast and fluorescent images as guides. The sample was left to infiltrate with resin for 1 h and polymerized at $+60°C$ overnight. Capsules were detached from the culture dish by dipping into liquid nitrogen. The MatTek grid was then visible on the surface of the epon block and it was used as guide to trim the block surface to contain the region of interest. Sections were cut with a diamond knife and post stained with uranyl acetate and lead citrate. A more comprehensive protocol for the CLEM method can be found in the materials and methods section of [37].

### 2.4 Cryofixation

Cells were cultured on 2 mm diameter sapphire discs or cultured directly on poly-L-lysine coated gold HPF carriers (Leica Microsystems). Cells were overlaid with 20% BSA in phosphate buffer (~1 min) and high pressure frozen using a Leica EM HPM100 (Leica Microsystems). The samples were transferred to the automated freeze substitution apparatus (Leica EM AFS) under liquid nitrogen, into a solution containing 2% osmium tetroxide, 0.3% uranyl acetate and 10% water in acetone, where the water was added first and frozen before adding the acetone, based on a method modified from Knoops et al. [49] (Fig. 5C). Samples were maintained at $-95°C$ for 4 h, slowly warmed to $-60°C$ (5° per hour) and maintained for 2 h, slowly warmed to $-30°C$ (5° per hour) and maintained for 2 h, and finally

slowly warmed to 0°C (5° per hour). Two washes with cold acetone were carried out at 0°C and cells were infiltrated in epon resin at room temperature for 2 h and polymerized at +60°C. Thin sectioning was carried out as described for CLEM.

### 3.1 Results

Collectively, these methods showcase the versatility of electron microscopy. Firstly, CLEM allows for spatial and temporal dynamic events to be captured at low magnification in fixed or living cells, respectively. The same organelles can then be located and viewed with the nano-structural resolution capabilities of the EM. SB-SEM as well as FIB-SEM has proven to be very effective systems in generating three-dimensional datasets with good ultrastructural resolution that lies between LM and EM, from large cell volumes (over 50 µm thick). These methods are helping to bridge the gap between LM and EM whereby various structures and organelles can only be fully understood when viewed in a three-dimensional space, in the context of their intracellular surroundings. Our laboratory has used the SB-SEM method to help determine which organelles have a close relationship with the phagophore during its biogenesis and the results have been very informative [11]. SB-SEM has confirmed that phagophores form in very close association with the ER in practically all cases observed (Fig. 1D, Suppl. movie 1). Additionally this method can be used to quantify the number of phagophores arising in close proximity to various organelles and we have found that it is not uncommon for the phagophore to be completely encapsulated by the ER, with simultaneous close communication with other organelles and structures including mitochondria and endosomes/ lysosomes (Fig. 1D, Suppl. movie 1) [11]. Lipid droplets are also routinely found with this method; however, the droplets seem to mainly communicate

20

with the ER and less frequently with the phagophore membrane directly (Fig. 1D, insert, Suppl. movie 1).

If adequate staining is introduced to optimize contrast in the pre-embedding immunoEM protocol, then there is potential that SB-SEM could be carried out on immunogold-labeled samples. For optimal contrast, selective reduction of osmium to form osmium deposits [44] or chemical reduction of osmium with potassium ferrocyanide produce the best contrast for biological membranes [50]. In our hands, SB-SEM was a very useful guide which allowed screening of the volumetric data of whole cells to help determine which organelles should be further targeted for dual-axis ET acquisition in order to verify whether the closely communicating organelles also made membrane connections with the phagophore at the nano-level [11].

Dual-axis ET is an essential tool for confirming direct membrane contacts between two organelles with minimal loss of information due to sectioning. Dual-axis ET was used to confirm that MCSs were present between the phagophore membrane and the ER membrane [13, 14] (Fig. 3, Suppl. movie 2), and that MCSs are very common [11]. Of note, the prevalence of MCSs is only now becoming more apparent with advancing technology which allows for ultrastructural three-dimensional visualization. With tomography data we have observed that the phagophore membrane is continuous with that of the ER (blue arrowheads in Fig. 3B). There is growing consensus that the phagophore nucleates from a subdomain on ER termed the omegasome [51]. In figure 3F we can also see that in the very top slices of the tomogram where the phagophore membrane has not fully materialized (green arrows), direct communication is observed between the ER (red arrow) and the phagophore membrane (green arrowhead) which indeed could be morphological

confirmation of the omegasome region of the ER. Further to this, it is not surprising that as the phagophore continues to grow and elongate it requires membrane input from additional sources in order not to exhaust the ER supply. Dual-axis ET can be used to help determine whether other organelles are also communicating with phagophores during their biogenesis [11]. However, it should be kept in mind that even though we have identified that MCS are a common phenomenon, verification on whether these membrane contacts also infer that lipid translocation is taking place requires further investigation.

Immunolabeling at the EM level has been very useful in the field of autophagy since morphological information can be complemented with ultrastructural localization of various antigens. ImmunoEM compatible antibodies are commercially available for the most commonly used autophagosome marker LC3 (microtubule-associated protein 1 light chain 3). In addition to autophagosomes and degradative autophagic vacuoles, LC3 is also present on phagophores. Depending on the orientation of the thin section, open phagophores can appear as closed double-membrane bound vesicles, similar to sealed autophagosomes. Both of these structures are also positive for LC3, thus we would need three-dimensional EM to definitely differentiate all phagophores from early autophagosomes. However, phagophores, unlike autophagosomes, are also positive for other markers including ATG12, ATG5, ATG16L1 and WIPI2, but these proteins may be difficult to label in immunoEM at least without overexpression. However, phagophores and early autophagosomes can be differentiated from later degradative autophagic vacuoles, which are also LC3 positive, by the morphology of the cytoplasmic contents: the content is morphologically intact in phagophores and early autophagosomes and partially degraded in degradative autophagic compartments. With the potential of

carrying out double or triple  labeling with the post-embedding immunoEM techniques or with the pre-embedding immunolabeling methods that use a combination of enzymatic and/or gold-based conjugates [52] autophagic compartments can be further elucidated. Since both autophagosomes and autolysosomes contain LC3 [53] (Fig. 4A-C) and lysosomes and autolysosomes express LAMP1 (lysosomal-associated membrane protein 1) (Fig. 4D), double labeling for these two markers will allow us to distinguish between lysosomes (LAMP1$^+$, LC3$^-$) and autolysosomes (LAMP1$^+$, LC3$^+$).

Finally, high-pressure cryofixation and AFS achieve rapid immobilization of the sample in the near native state. This method revealed that autophagosomes do not exhibit a wide empty cleft between the two limiting membranes [43] (Fig. 5D). Further, this method can be used to determine whether MCSs are present between phagophores and other organelles.  Although trouble shooting the AFS medium to give the best contrast can be laborious, particularly when trying to get good membrane contrast for phagophores and autophagosomes, we found that a solution containing 2% osmium tetroxide, 0.3% uranyl acetate and 10% water in acetone, yielded the best results and has allowed sampling of HPF-AFS sections for dual-axis ET.

### 4.1 Concluding remarks

Taken together, we and others have shown that the EM is a very valuable and multifunctional instrument in the study of autophagy. It has the capability of providing ultrastructural information from whole cell volumes, as well as nano-structural resolution to show intricate detail such as membrane contact sites. Further to this, functional studies can be performed whereby the same cells and

23

organelles can be first imaged in a living state using light microscopy, followed by fixation and high-resolution imaging at EM where the precise sub-cellular localization of antigens can be determined. Finally, the physiological state of cells and organelles can be observed when cells are immobilized with the application of high- pressure cryofixation.  All of these aforementioned methods for studying autophagy come with the obvious advantage that is only obtained when using EM, that is, ultrastructural resolution revealing the intracellular context.

**Acknowledgments**

**References**

[1] C.J. Peddie, L.M. Collinson, Exploring the third dimension: volume electron microscopy comes of age, Micron 61 (2014) 9-19.

[2] K.E. Carr, P.G. Toner, K.M. Saleh, Scanning electron microscopy, Histopathology 6 (1982) 3-24.

[3] T. Starborg, N.S. Kalson, Y. Lu, A. Mironov, T.F. Cootes, D.F. Holmes, K.E. Kadler, Using transmission electron microscopy and 3View to determine collagen fibril size and three-dimensional organization, Nature Protocols 8 (2013) 1433-1448.

[4] L. Hughes, C. Hawes, S. Monteith, S. Vaughan, Serial block face scanning electron microscopy-the future of cell ultrastructure imaging, Protoplasma 251 (2014) 395-401.

[5] S.B. Leighton, SEM images of block faces, cut by a miniature microtome within the SEM - a technical note, Scan. Electron Microsc. 2 (1981) 73-76.

[6] W. Denk, H. Horstmann, Serial block-face scanning electron microscopy to reconstruct three-dimensional tissue nanostructure, PLoS Biol. 2 (2004) e329.

[7] D.N. Mastronarde, Automated electron microscope tomography using robust prediction of specimen movements, J. Struct. Biol. 152 (2005) 36-51.

[8] G. Knott, H. Marchman, D. Wall, B. Lich, Serial section scanning electron microscopy of adult brain tissue using focused ion beam milling, J. Neurosci. 28 (2008) 2959-2964.

[9] A. Merchan-Perez, J.R. Rodriguez, L. Alonso-Nanclares, A. Schertel, J. Defelipe, Counting Synapses Using FIB/SEM Microscopy: A True Revolution for Ultrastructural Volume Reconstruction, Front. Neuroanat. 3 (2009) 18.

[10] S.J. Park, A. Schertel, K.E. Lee, S.S. Han, Ultra-structural analysis of the brain in a Drosophila model of Alzheimer's disease using FIB/SEM microscopy, Microscopy 63 (2014) 3-13.

[11] J. Biazik, P. Ylä-Anttila, H. Vihinen, E. Jokitalo, E.L. Eskelinen, Ultrastructural relationship of the phagophore with surrounding organelles, Autophagy (in press).

[12] S.C. Helle, G. Kanfer, K. Kolar, A. Lang, A.H. Michel, B. Kornmann, Organization and function of membrane contact sites, Biochim. Biophys. Acta 1833 (2013) 2526-2541.

[13] M. Hayashi-Nishino, N. Fujita, T. Noda, A. Yamaguchi, T. Yoshimori, A. Yamamoto, A subdomain of the endoplasmic reticulum forms a cradle for autophagosome formation, Nat. Cell Biol. 11 (2009) 1433-1437.

[14] P. Yla-Anttila, H. Vihinen, E. Jokitalo, E.L. Eskelinen, 3D tomography reveals connections between the phagophore and endoplasmic reticulum, Autophagy 5 (2009) 1180-1185.

[15] M. Hamasaki, N. Furuta, A. Matsuda, A. Nezu, A. Yamamoto, N. Fujita, H. Oomori, T. Noda, T. Haraguchi, Y. Hiraoka, A. Amano, T. Yoshimori, Autophagosomes form at ER-mitochondria contact sites, Nature 495 (2013) 389-393.

[16] K. Hanada, K. Kumagai, N. Tomishige, M. Kawano, CERT and intracellular trafficking of ceramide, Biochim. Biophys. Acta 1771 (2007) 644-653.

[17] J. Frank, Electron tomography: methods for three-dimensional visualization of structures in the cell, Springer, New York, 2006.

 [18] D.N. Mastronarde, Dual-axis tomography: an approach with alignment methods that preserve resolution, J. Struct. Biol. 120 (1997) 343-352.

[19] E.L. Eskelinen, To be or not to be? Examples of incorrect identification of autophagic compartments in conventional transmission electron microscopy of mammalian cells, Autophagy 4 (2008) 257-260.

[20] P. Ylä-Anttila, H. Vihinen, E. Jokitalo, E.L. Eskelinen, Monitoring autophagy by electron microscopy in Mammalian cells, Methods Enzymol. 452 (2009) 143-164.

[21] R.W. Burry, D.D. Vandre, D.M. Hayes, Silver enhancement of gold antibody probes in pre-embedding electron microscopic immunocytochemistry, J. Histochem. Cytochem. 40 (1992) 1849-1856.

[22] J.M. Robinson, T. Takizawa, D.D. Vandre, Enhanced labeling efficiency using ultrasmall immunogold probes: immunocytochemistry, J. Histochem. Cytochem. 48 (2000) 487-492.

[23] K.T. Tokuyasu, Application of cryoultramicrotomy to immunocytochemistry, J. Microsc. 143 (1986) 139-149.

[24] J. Griffith, M. Mari, A. De Maziere, F. Reggiori, A cryosectioning procedure for the ultrastructural analysis and the immunogold labelling of yeast Saccharomyces cerevisiae, Traffic 9 (2008) 1060-1072.

[25] M.A. Karreman, E.G. Van Donselaar, A.V. Agronskaia, C.T. Verrips, H.C. Gerritsen, Novel contrasting and labeling procedures for correlative microscopy of thawed cryosections, J. Histochem. Cytochem. 61 (2013) 236-247.

[26] W. Liou, H.J. Geuze, J.W. Slot, Improving structural integrity of cryosections for immunogold labeling, Histochem. Cell Biol. 106 (1996) 41-58.

[27] T. Takizawa, C.L. Anderson, J.M. Robinson, A new method to enhance contrast of ultrathin cryosections for immunoelectron microscopy, J. Histochem. Cytochem. 51 (2003) 31-39.

[28] P. Webster, H. Schwarz, G. Griffiths, Preparation of cells and tissues for immuno EM, Methods Cell Biol. 88 (2008) 45-58.

[29] J.M. Robinson, T. Takizawa, D.D. Vandre, R.W. Burry, Ultrasmall immunogold particles: important probes for immunocytochemistry, Microsc. Res. Tech. 42 (1998) 13-23.

[30] D. Zeuschner, W.J. Geerts, E. van Donselaar, B.M. Humbel, J.W. Slot, A.J. Koster, J. Klumperman, Immuno-electron tomography of ER exit sites reveals the existence of free COPII-coated transport carriers, Nat. Cell Biol. 8 (2006) 377-383.

[31] M. Mari, W.J. Geerts, F. Reggiori, Immuno- and correlative light microscopy-electron tomography methods for 3D protein localization in yeast, Traffic 15 (2014) 1164-1178.

[32] E. van Donselaar, G. Posthuma, D. Zeuschner, B.M. Humbel, J.W. Slot, Immunogold labeling of cryosections from high-pressure frozen cells, Traffic 8 (2007) 471-485.

[33] V. Kondylis, H.E. van Nispen Tot Pannerden, S. van Dijk, T. Ten Broeke, R. Wubbolts, W.J. Geerts, C. Seinen, T. Mutis, H.F. Heijnen, Endosome-mediated autophagy: an unconventional MIIC-driven autophagic pathway operational in dendritic cells, Autophagy 9 (2013) 861-880.

[34] R.S. Polishchuk, E.V. Polishchuk, A. Luini, Visualizing live dynamics and ultrastructure of intracellular organelles with preembedding correlative light-electron microscopy, Methods Cell Biol. 111 (2012) 21-35.

[35] J. Lippincott-Schwartz, T.H. Roberts, K. Hirschberg, Secretory protein trafficking and organelle dynamics in living cells, Ann. Rev. Cell Dev. Biol. 16 (2000) 557-589.

[36] C. van Rijnsoever, V. Oorschot, J. Klumperman, Correlative light-electron microscopy (CLEM) combining live-cell imaging and immunolabeling of ultrathin cryosections, Nat. Meth. 5 (2008) 973-980.

[37] M. Razi, S.A. Tooze, Correlative light and electron microscopy, Meth. Enzymol. 452 (2009) 261-275.

[38] A. Orsi, M. Razi, H.C. Dooley, D. Robinson, A.E. Weston, L.M. Collinson, S.A. Tooze, Dynamic and transient interactions of Atg9 with autophagosomes, but not membrane integration, are required for autophagy, Mol. Biol. Cell 23 (2012) 1860-1873.

[39] T. Takizawa, J.M. Robinson, FluoroNanogold is a bifunctional immunoprobe for correlative fluorescence and electron microscopy, J. Histochem. Cytochem. 48 (2000) 481-486.

[40] X. Shu, V. Lev-Ram, T.J. Deerinck, Y. Qi, E.B. Ramko, M.W. Davidson, Y. Jin, M.H. Ellisman, R.Y. Tsien, A genetically encoded tag for correlated light and electron microscopy of intact cells, tissues, and organisms, PLoS Biol. 9 (2011) e1001041.

[41] D. Boassa, M.L. Berlanga, M.A. Yang, M. Terada, J. Hu, E.A. Bushong, M. Hwang, E. Masliah, J.M. George, M.H. Ellisman, Mapping the subcellular distribution of alpha-synuclein in neurons using genetically encoded probes for correlated light and electron microscopy: implications for Parkinson's disease pathogenesis, J. Neurosci. 33 (2013) 2605-2615.

[42] J. Dubochet, M. Adrian, J.J. Chang, J.C. Homo, J. Lepault, A.W. McDowall, P. Schultz, Cryo-electron microscopy of vitrified specimens, Quar. Rev. of Biophys. 21 (1988) 129-228.

[43] A.L. Kovacs, Z. Palfia, G. Rez, T. Vellai, J. Kovacs, Sequestration revisited: integrating traditional electron microscopy, de novo assembly and new results, Autophagy 3 (2007) 655-662.

[44] C.R. Hawes, B.E. Juniper, J.C. Horne, Low and high voltage electron microscopy of mitosis and cytokinesis in maize roots, Planta 152 (1981) 397-407.

[45] M. Puhka, M. Joensuu, H. Vihinen, I. Belevich, E. Jokitalo, Progressive sheet-to-tubule transformation is a general mechanism for endoplasmic reticulum partitioning in dividing mammalian cells, Mol. Biol. Cell 23 (2012) 2424-2432.

[46] J.R. Kremer, D.N. Mastronarde, J.R. McIntosh, Computer visualization of three-dimensional image data using IMOD, J. Struct. Biol. 116 (1996) 71-76.

[47] K. Tabata, M. Hayashi-Nishino, T. Noda, A. Yamamoto, T. Yoshimori, Morphological analysis of autophagy, Methods Mol. Biol. 931 (2013) 449-466.

[48] A. Yamamoto, R. Masaki, Pre-embedding nanogold silver and gold intensification, Methods Mol. Biol. 657 (2010) 225-235.

[49] K. Knoops, M. Kikkert, S.H. Worm, J.C. Zevenhoven-Dobbe, Y. van der Meer, A.J. Koster, A.M. Mommaas, E.J. Snijder, SARS-coronavirus replication is supported by a reticulovesicular network of modified endoplasmic reticulum, PLoS Biol. 6 (2008) e226.

[50] E. Schnepf, K. Hausmann, W. Herth, The osmium tetroxide-potassium ferrocyanide (OsFeCN) staining technique for electron microscopy: a critical evaluation using ciliates, algae, mosses, and higher plants, Histochemistry 76 (1982) 261-271.

[51] T. Uemura, M. Yamamoto, A. Kametaka, Y.S. Sou, A. Yabashi, A. Yamada, H. Annoh, S. Kametaka, M. Komatsu, S. Waguri, A cluster of thin tubular structures mediates transformation of the endoplasmic reticulum to autophagic isolation membrane, Mol. Cell Biol. 34 (2014) 1695-1706.

[52] C.D. Paspalas, P.S. Goldman-Rakic, Microdomains for dopamine volume neurotransmission in primate prefrontal cortex, J. Neurosci. 24 (2004) 5292-5300.

[53] L. Yu, C.K. McPhee, L. Zheng, G.A. Mardones, Y. Rong, J. Peng, N. Mi, Y. Zhao, Z. Liu, F. Wan, D.W. Hailey, V. Oorschot, J. Klumperman, E.H. Baehrecke, M.J. Lenardo, Termination of autophagy and reformation of lysosomes regulated by mTOR, Nature 465 (2010) 942-946.

**Figure Legends**

**Figure 1**

**Volumetric data with ultrastructural resolution.** SB-SEM instrumentation (*Photos courtesy of the EM Unit, The University of Helsinki)* showing the SEM chamber with inbuilt microtome (A-C). A diagram of the cutting mechanism and block face produced with this method is shown (B, *insert*) as well as a side- and top view of the three-dimensional model constructed from the SB-SEM slices (D). The volumetric data was obtained from over 4 µm in the z plane. The model shows a phagophore (green-ph) in close communication with mitochondria (brown-m), the ER (red-ER), lipid droplets (blue-L) and an autophagosome (yellow-Au).

**Figure 2**

**Segmentation of SB-SEM volumetric data.** The 40-nm 'sections', or levels of the block face (numbered in the lower right) show how the segmentation of the open c-shaped phagophore membrane was carried out to produce the three-dimensional model of the phagophore (green) from panel number 46 and onwards.

**Figure 3**

**Nano-structural detail revealed with dual-axis ET.** Tomographic slices (1.6-2 nm thick) showing a phagophore forming in close proximity to the plasma membrane (A, pink arrow) and the corresponding 3D model (D, H). The electron dense c-shaped phagophore is depicted as lying in between the inner ER (red *) and the outer ER (yellow **). Yellow arrows depict contacts between the phagophore and the outer ER

31

(A, E, G-H, *inserts*) and red arrows indicate areas of contact between the phagophore and the inner ER (B-C, F-H, *inserts*). Black arrowhead indicates membrane continuity between the inner and the outer ER (C-D). Blue arrowheads indicate membrane continuity between the phagophore membrane and the ER in the 1.6 nm slice (B) and the green arrowhead depicts the closely apposed membranes of the phagophore (G). The green arrows show a region of the phagophore in the very top slices of the tomogram where the phagophore membrane has not been fully laid down yet (F).

**Figure 4**

**Pre-embedding immunolabeling.** When using 4% paraformaldehyde as an initial fixative, our results indicate good preservation of antigenicity when using anti-LC3 to label phagophores and autophagosomes (A-C, white arrowheads) or anti-LAMP-1 to label lysosomes and late endosomes (D, black arrowheads). The primary antibodies were detected using secondary antibodies conjugated with 1.4-nm gold followed by silver enhancement protocol. This method also preserves ultrastructural information such as vesicles lying close to the plasma membrane (A, black arrows), mitochondrial cristae (A-D, m), and thin Golgi complex cisternae (C, Go). A clear distinction of the nuclear envelope is also evident (C, white arrows).

**Figure 5**

**High-pressure cryofixation reveals a clear distinction of the double membranes of autophagic compartments**. Cells can be cultured on sapphire discs
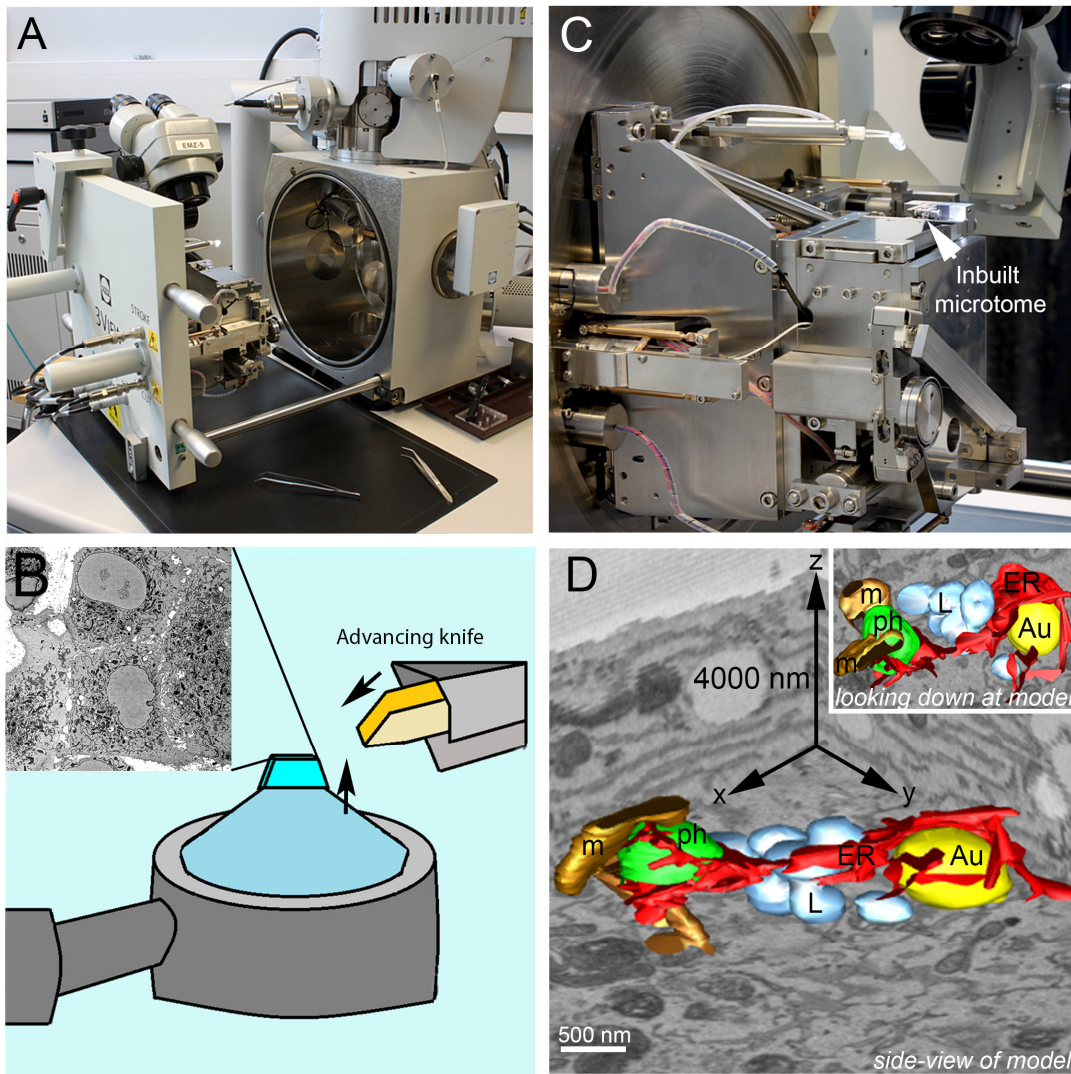
that fit inside the HPF specimen carrier, as well as directly on poly-L-lysine coated

HPF carriers (A). A series of commercially available HPF units are available; panel B

shows our Leica EM HPM100 (Leica Microsystems). The order in which you add the

different freeze-substitution media components may affect membrane contrast, we

have found that freezing the water component first, before adding the remaining

medium, works well and this keeps the water drop at the bottom of the cryovial. The

HPF specimen carrier should then be dropped under liquid nitrogen onto the frozen

FS medium vial that is sitting partially submerged in liquid nitrogen, just when the top

layer of the medium begins to melt (C). Ultrastructural information is greatly

preserved, as is evident in panel D, which shows the clear distinction of the double

membranes of an autophagosome (*insert*). The mitochondrion inside the

autophagosome also has well preserved cristae (m), which is also indicative of a

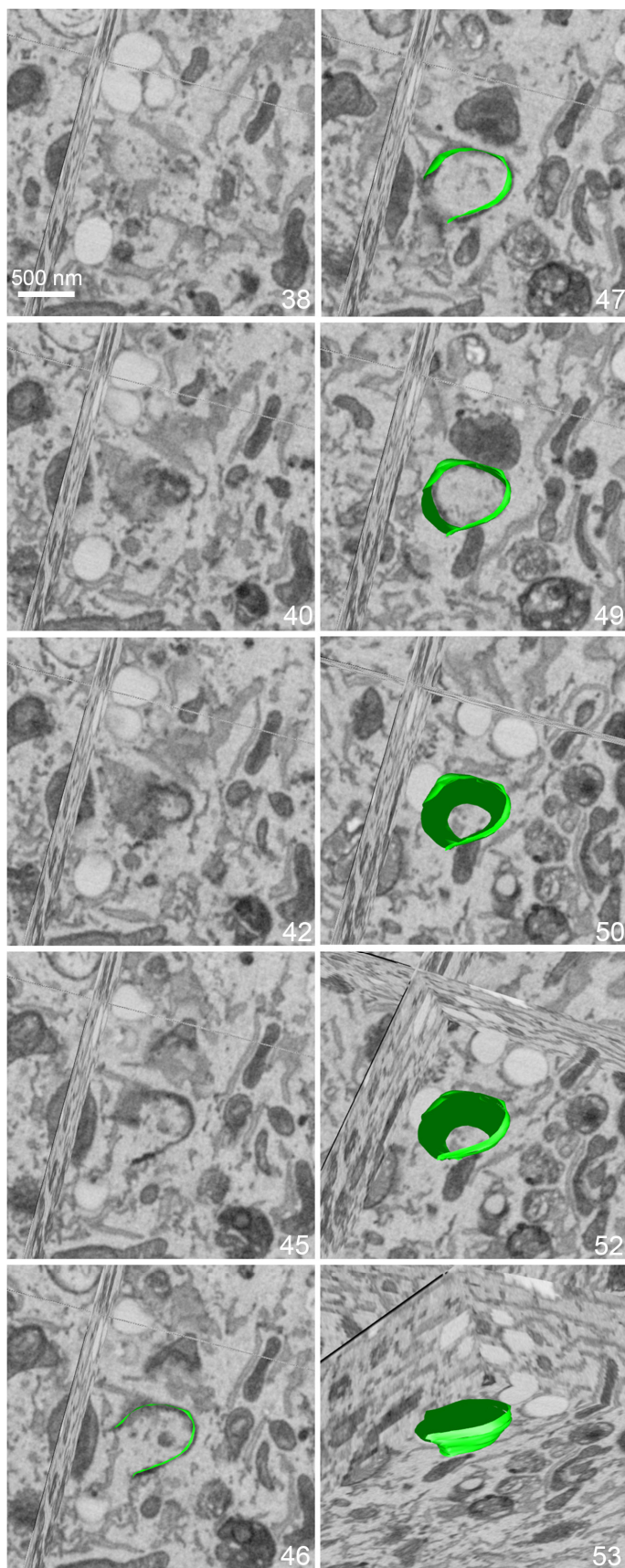very early autophagic compartment.

**Supplementary movie 1**

**SB-SEM slices and 3D model of the still image depicted in Figure 1D** showing

the close communication between  the phagophore membrane (green) and two

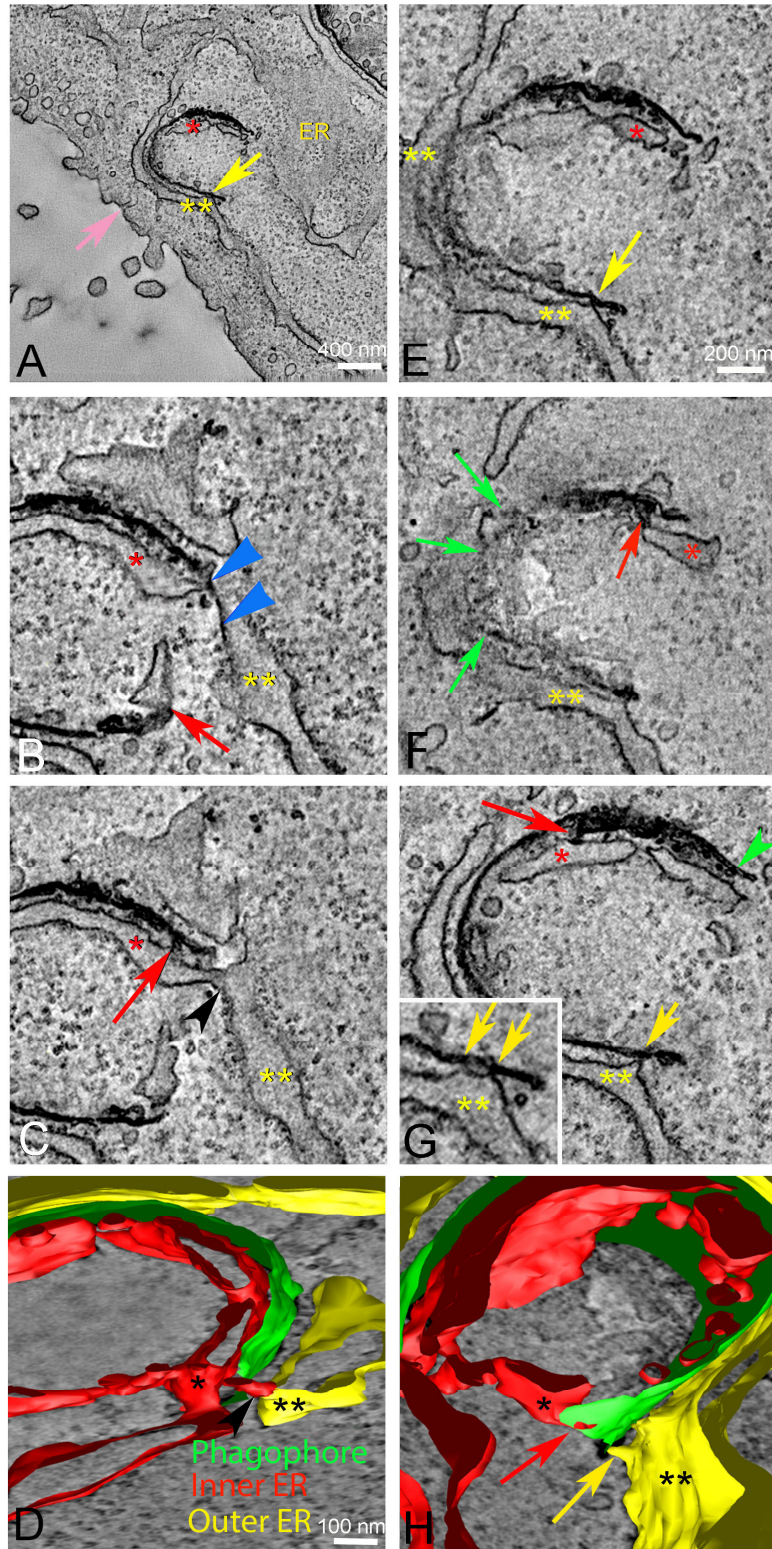mitochondria (brown), the ER (red), lipid droplets (blue) and an autophagosome

(yellow).

**Supplementary movie 2**

**Movie of the tomographic slices and 3D model of the phagophore which is

depicted in Figure 3.** The dark double membrane of the phagophore (green) is

seen to be lying in between two ER sheets (red and yellow). The plasma membrane
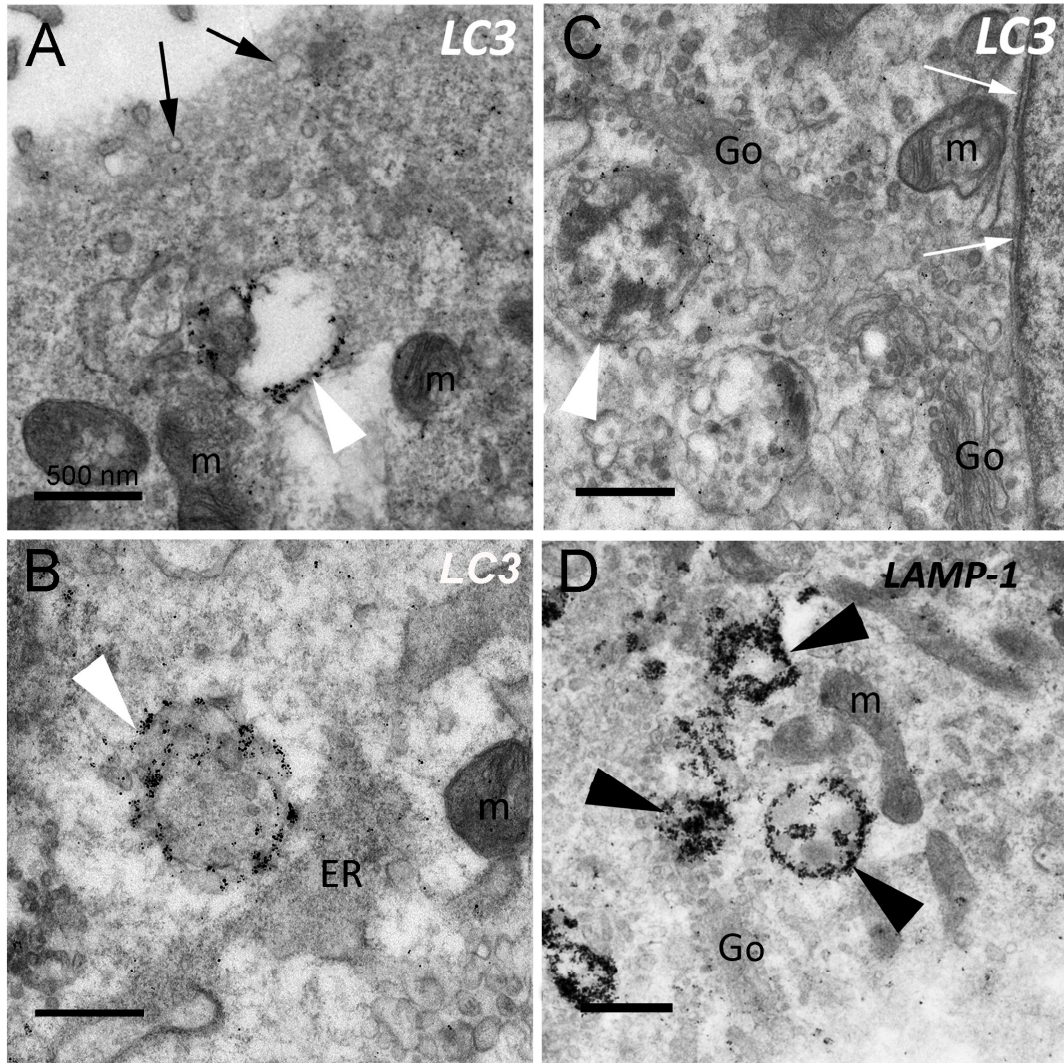
is depicted pink.

33

A

B

Advancing knife

C

Inbuilt microtome

D

z

m
ph
L
ER
Au

looking down at model

4000 nm

x    y

m
ph
L
ER
Au

500 nm

side-view of model

A

3 mm

B

C

HPF carrier dropped on
frozen FS medium as it
starts to melt

Frozen FS medium in
cryovial

Add drop of water first

D

m

500 nm